

Claudin-16 Deficiency Impairs Tight Junction Function in Ameloblasts, Leading to Abnormal Enamel Formation

Claire Bardet,¹ Frédéric Courson,^{2*} Yong Wu,^{1,3*} Mayssam Khaddam,¹ Benjamin Salmon,^{1,2} Sandy Ribes,¹ Julia Thumfart,⁴ Paulo M Yamaguti,⁵ Gael Y Rochefort,¹ Marie-Lucile Figueures,⁶ Tilman Breiderhoff,⁴ Alejandro Garcia-Castaño,⁷ Benoit Vallée,⁸ Dominique Le Denmat,¹ Brigitte Baroukh,¹ Thomas Guilbert,⁹ Alain Schmitt,¹⁰ Jean-Marc Massé,¹⁰ Dominique Bazin,¹¹ Georg Lorenz,¹² Maria Morawietz,¹² Jianghui Hou,¹³ Patricia Carvalho-Lobato,¹⁴ Maria Cristina Manzanares,¹⁴ Jean-Christophe Fricain,¹⁵ Deborah Talmud,¹⁶ Renato Demontis,¹⁷ Francisco Neves,¹⁸ Delphine Zenaty,¹⁹ Ariane Berdal,⁶ Andreas Kiesow,¹² Matthias Petzold,¹² Suzanne Menashi,⁸ Agnes Linglart,²⁰ Ana Carolina Acevedo,⁵ Rosa Vargas-Poussou,⁷ Dominik Müller,⁴ Pascal Houillier,^{6,21} and Catherine Chaussain^{1,2}

¹EA 2496, Laboratory Orofacial Pathologies, Imaging and Biotherapies, Dental School Paris Descartes University, Sorbonne Paris Cité, France

²Department of Odontology, AP-HP, and Reference Center for Rare Diseases of the Metabolism of Calcium and Phosphorus, Nord Val de Seine Hospital, Bretonneau, France

³Department of Oral and Cranio-maxillofacial Science, Ninth People's Hospital, Shanghai Jiao Tong University School of Medicine, Shanghai Key Laboratory of Stomatology, Shanghai, China

⁴Department of Pediatric Nephrology, Charité University School of Medicine, Berlin, Germany

⁵Division of Dentistry, Oral Care Center for Inherited Diseases, University Hospital of Brasilia, Faculty of Health Sciences, University of Brasilia (UnB), Brasilia, Brazil

⁶INSERM UMR 1138, Cordeliers Research Center, Paris-Diderot, Pierre et Marie Curie and Paris Descartes Universities, CNRS ERL 8228, Paris, France

⁷Department of Genetics, AP-HP, and Reference Center of Children and Adult Renal Hereditary Diseases (MARHEA), European Hospital Georges Pompidou, Paris, France

⁸Laboratory CRRET, Paris-Est University, CNRS, Créteil, France

⁹Cochin Institute, Plate-Forme d'Imagerie Photonique, INSERM U1016, CNRS UMR8104, Paris Descartes University Sorbonne Paris Cité, Paris, France

¹⁰Cochin Institute, Transmission Electron Microscopy Platform, INSERM U1016, CNRS UMR8104, Paris Descartes University Sorbonne Paris Cité, Paris, France

¹¹Laboratoire de Physique des Solides, CNRS, Paris Sud University, Orsay, and LCMCP-UPMC, Collège de France, Paris, France

¹²Fraunhofer Institute for Mechanics of Materials IWM, Halle, Germany

¹³Division of Renal Diseases, Washington University School of Medicine, St. Louis, MO, USA

¹⁴Human Anatomy and Embryology, Health University of Barcelona Campus-Bellvitge, University of Barcelona, Barcelona, Spain

¹⁵CHU Bordeaux, Dental School, U1026 Tissue Bioengineering, University of Bordeaux/Inserm, Bordeaux, France

¹⁶Department of Pediatrics, Centre Hospitalier Régional (CHR) d'Orléans, Orleans, France

¹⁷GHPSO, Creil, France

¹⁸Laboratory of Molecular Pharmacology, Faculty of Health Sciences, University of Brasilia (UNB), Brasilia, Brazil

¹⁹Department of Pediatric Endocrinology, AP-HP, Paris Diderot University, Robert Debré Hospital, Paris, France

²⁰Department of Pediatric Endocrinology, AP-HP, Paris Sud University, School of Medicine, and Reference Center for Rare Diseases of the Metabolism of Calcium and Phosphorus, Paris, France

²¹Department of Physiology, AP-HP, and Reference Center of Children and Adult Renal Hereditary Diseases (MARHEA), Georges Pompidou European Hospital, Paris, France

ABSTRACT

Claudin-16 protein (CLDN16) is a component of tight junctions (TJ) with a restrictive distribution so far demonstrated mainly in the kidney. Here, we demonstrate the expression of CLDN16 also in the tooth germ and show that claudin-16 gene (*CLDN16*) mutations result in amelogenesis imperfecta (AI) in the 5 studied patients with familial hypomagnesemia with hypercalciuria and nephrocalcinosis (FHHNC). To investigate the role of CLDN16 in tooth formation, we studied a murine model of FHHNC and showed

Received in original form May 15, 2015; revised form September 28, 2015; accepted September 29, 2015. Accepted manuscript online Month 00, 2015.

Address correspondence to: Catherine Chaussain, DDS, PhD, EA 2496, Dental School University Paris Descartes, 1 Rue Maurice Arnoux 92120, Montrouge, France. E-mail: catherine.chaussain@parisdescartes.fr; Pascal Houillier, MD, PhD, Cordeliers Research Center, 15 Rue de l'École de Médecine 75006, Paris, France. E-mail: pascal.houillier@inserm.fr

*FC and YW contributed equally to this work.

Additional Supporting Information may be found in the online version of this article.

Journal of Bone and Mineral Research, Vol. xx, No. xx, Month 2015, pp 1–16

DOI: 10.1002/jbmr.2726

© 2015 American Society for Bone and Mineral Research

that CLDN16 deficiency led to altered secretory ameloblast TJ structure, lowering of extracellular pH in the forming enamel matrix, and abnormal enamel matrix protein processing, resulting in an enamel phenotype closely resembling human AI. This study unravels an association of FHHNC owing to *CLDN16* mutations with AI, which is directly related to the loss of function of CLDN16 during amelogenesis. Overall, this study indicates for the first time the importance of a TJ protein in tooth formation and underlines the need to establish a specific dental follow-up for these patients. © 2015 American Society for Bone and Mineral Research.

KEY WORDS: AMELOGENESIS IMPERFECTA (AI); FAMILIAL HYPOMAGNESEMIA WITH HYPERCALCIURIA AND NEPHROCALCINOSIS (FHHNC); SECRETORY AMELOBLASTS; pH; MMP-20

Introduction

The claudin (CLDN) components of the tight junctions (TJ) were shown to determine the size and ion specificity of individual TJ.⁽¹⁾ Among them, claudin-16 (CLDN16, initially called paracellin-1)⁽²⁾ is expressed primarily in the thick ascending limb of Henle's loop in the kidney, where, in association with claudin-19, it forms cation-selective pores allowing reabsorption of Ca²⁺ and Mg²⁺.⁽¹⁻³⁾ Mutations in the claudin genes *CLDN16* or *CLDN19* were shown to cause familial hypomagnesemia with hypercalciuria (HC) and nephrocalcinosis (NC) (FHHNC; OMIM 248250 and OMIM 248190, respectively), a rare kidney condition characterized by renal Ca²⁺ and Mg²⁺ wasting evolving to renal insufficiency.^(2,4)

Clinical cases describing the association of kidney disease and amelogenesis imperfecta (AI) have been described as early as 1972.^(5,6) AI is defined as a group of genetic disorders that affect to varying degrees tooth enamel formation of all or nearly all the teeth in either the primary or permanent dentition or both.⁽⁷⁾ The resulting enamel can be classified as hypoplastic (thin but normally calcified), hypocalcified (soft), or hypomatatured (reduced mineral density and brown discolorations).^(7,8) AI may occur as an isolated condition that only affects enamel (nonsyndromic AI) or in association with abnormalities in other tissues (syndromic conditions associated with AI).⁽⁹⁾ In 2006, the association between FHHNC and enamel disorder has been reported based on the oral examination of two Chinese sisters with FHHNC, who both showed marked AI with severe enamel hypoplasia.⁽¹⁰⁾ This important finding had not been pursued since, whereas another association of kidney condition and AI, the enamel renal syndrome (ERS), has recently raised a great interest.⁽¹¹⁻¹³⁾ ERS, which is caused by bi-allelic mutations in *FAM20A* encoding a Golgi kinase,^(14,15) was first described as a distinct phenotypic entity (ERS, OMIM 204690) but was later associated with gingival fibromatosis syndrome (AIGFS, OMIM 614253).^(16,17) Unlike the association of FHHNC and AI reported by Cetrullo and colleagues,⁽¹⁰⁾ ERS is characterized by ectopic calcifications of the dental pulp and gingiva attesting the difference between these two disorders.

During enamel development, ameloblasts progress through defined developmental stages requiring cell-cell contact, detachment, cell reattachment, and intercellular communication and TJ have been shown to be essential in these processes.^(18,19) Several *CLDN* genes are expressed at various developmental stages in the tooth germ where they were proposed to modulate TJ properties.^(1,18,20) However, to date, *CLDN16* expression has not yet been reported in the tooth. Because AI has already been associated with FHHNC,⁽¹⁰⁾ we thought to determine whether *CLDN16* mutations were responsible for abnormal enamel formation in this disorder. In that purpose, we characterized the oral phenotype of 5 unrelated patients with autosomal recessive FHHNC owing to *CLDN16* mutations,^(4,21,22) as well as *Cldn16*^{-/-} mice, the murine

model of the disorder.⁽²³⁾ We demonstrate the expression of CLDN16, so far mainly described in the kidney, in the forming tooth and show that mutations in this gene resulted in enamel abnormalities both in FHHNC patients and in *Cldn16*^{-/-} mice.

Materials and Methods

Genetic studies

Genomic DNA was extracted by standard methods from peripheral blood samples after informed consent was obtained from each participating subject (or the parents of the younger children). For patients 1 to 4, ethical agreement was received in the frame of the diagnosis Centre for Molecular Diagnosis of Familial Hypomagnesemia and Hypercalciuria by the Laboratory of Molecular Genetics (CHU Paris IdF Ouest - HEGP Hôpital Européen Georges Pompidou, France) accredited by the French Agency of Biomedicine (agreement AFSB1330617S for RVP), and for patient 5 by the Oral Care Center for Inherited Diseases, Brasilia-Brazil (CONEP 1440/2001). Mutation analyses was performed based on PCR amplification followed by sequencing as previously described^(21,24) (primers available on request) on an ABI Prism 3730XL DNA Analyzer (Perkin Elmer Applied Biosystems, Foster City, CA, USA). Mutations were interpreted, and the degree of amino acid conservation between orthologs and Grantham distance was assessed with Alamut v.2.0 software (Interactive Biosoftware, Rouen, France; <http://www.interactivebiosoftware.com/>). Complementary analyses were performed with: SIFT (<http://www.Blocks.fhcrc.org/sift/SIFT.html>), PolyPhen-2 (<http://genetics.bwh.harvard.edu/pph/>), MutationTaster (<http://www.mutationtaster.org/>).

Oral examination of patients with FHHNC owing to *CLDN16* mutations

Clinical examination was performed by senior dental practitioners and completed by intraoral X-rays and panoramic radiograph. The presence of enamel defects was determined by visual examination of tooth surfaces and the abnormalities were classified according to AI classifications.^(7,8) For patients with unerupted permanent teeth, a 3D cone beam CT (CBCT) exam was performed.

Cldn16^{-/-} mice

Cldn16^{-/-} mice were obtained as previously described.⁽²³⁾ Heterozygous breeding was carried out and tail snips were collected for genotyping. DNA was extracted from the snips using DNeasy Blood and Tissue Kit (Qiagen, Paris, France) and the genotype was determined by PCR using primers for *Cldn16* gene.⁽²³⁾ Offspring with the *Cldn16* gene null mutant (*Cldn16*^{-/-}) phenotype were maintained under the same conditions as those for the wild-type (WT) mice. Postnatal day 3 (PN3), postnatal day 4 (PN4), and 3-month-old littermate *Cldn16*^{+/+} (WT) and

Cldn16^{-/-} mice were examined in this study. Before death, blood pH was measured in vigil 3-month-old littermate WT and *Cldn16*^{-/-} mice ($n = 8$ per group) using epoc pH Reader device (Alere, Atlanta, GA, USA) (ethical agreement number: CE5/2012/084). Chemical methods were used for mice euthanization according to the ethical protocol approved by the Animal Care Committee of French Veterinary Services (DPP Haut de Seine, France: agreement number C-9204901).

All mice were housed in standard conditions of temperature ($23 \pm 2^\circ\text{C}$) in a light-controlled environment, with unlimited access to water and standard pelleted food (rodent diet 3800PMS10, Provimi Kliba, Kaiseraugst, Switzerland).

Transmission electron microscopy (TEM)

Mandibles of PN3 WT and *Cldn16*^{-/-} littermate mice ($n = 3$ per group) were analyzed by conventional transmission electron microscopy (TEM). Heads were fixed in 2% (w/v) glutaraldehyde in 0.15 M cacodylate buffer, pH 7.4, overnight at 4°C . After post-fixation in 2% OsO₄ for 1 hour and dehydration in graded ethanol series at 4°C , the samples were embedded in Epon 812 (Fluka, Sigma-Aldrich, St. Louis, MO, USA). Semithin sections were stained with toluidine blue and fuchsin. After washing, the sections were dried and mounted in Eukitt. Ultrathin sections of undecalcified mandibles were stained with uranyl acetate and lead citrate and were examined with a JEOL 1011 electron microscope.

Immunofluorescence analysis

Lower jaws of PN3 WT and *Cldn16*^{-/-} littermate mice ($n = 6$ per group) were embedded in OCT compound before frozen sectioning. Seven-micrometer-thick undecalcified frozen tissue sections were prepared. For CLDN16 and ZO-1 immunolocalization, rabbit polyclonal CLDN16 antibody⁽³⁾ and goat monoclonal ZO-1 antibody (Santa Cruz Biotechnology, Dallas, TX, USA) were used at 1/200 and 1/50 dilution, respectively. Background activity was blocked at room temperature for 90 minutes in 1% bovine serum albumin (BSA) in PBS. A goat anti-rabbit immunoglobulin-G alexa Fluor 488 (Invitrogen, Carlsbad, CA, USA) and a donkey anti-goat immunoglobulin-G TRITC (Abcam, Cambridge, MA, USA) were used, respectively, 1 hour at room temperature in a dark chamber. Nuclei were stained with Dapi solution at 1/4000 (Invitrogen) for 3 minutes. Images were merged using Image J software (NIH, Bethesda, MD, USA).

To examine the signal distribution of CLDN16 immunostaining in WT and *Cldn16*^{-/-} mice, a Yokogawa csu X1 Spinning Disk coupled with a DMI6000B Leica microscope and oil objectives (Olympus) were used. Acquisitions were made with MetaMorph 7 software. Identical imaging settings were used for all acquisitions. Analyses were performed using ImageJ Colocalization plugin (<http://imagej.nih.gov/ij/>). Same threshold levels were used for both WT and *Cldn16*^{-/-} cases.

Immunohistochemistry

The mandibles of PN3 and PN4 WT and *Cldn16*^{-/-} littermate mice ($n = 6$ per group) were fixed overnight in a 4% paraformaldehyde solution. PN4 samples were decalcified overnight at 4°C in 4.13% EDTA. The PN3 and PN4 samples were then progressively dehydrated and embedded in Paraplast (Oxford Labware, St. Louis, MO, USA). Seven-micrometer-thick paraffin tissue sections were prepared (sagittal sections of PN3 mandibles for incisor analysis, frontal sections of PN4 mandibles

for molar germ analysis), deparaffined, and rehydrated. Endogenous peroxidases were blocked in 0.4% hydrogen peroxide in methanol. After extended rinsing in PBS, background activity was blocked at room temperature for 90 minutes in 1% bovine serum albumin (BSA) in PBS. Goat polyclonal enamelin antibody (Santa Cruz Biotechnology) and rabbit polyclonal amelogenin (Santa Cruz Biotechnology) and MMP-20 (N-terminal MMP-20 antibody, Sigma-Aldrich) antibodies were used at 1/50, 1/200, and 1/100 dilution, respectively. Sections were treated overnight in a moist chamber at 4°C and further incubated for 90 minutes with a polyclonal swine anti-rabbit immunoglobulin-G peroxidase conjugate or a polyclonal rabbit anti-goat immunoglobulin-G peroxidase conjugate (Dako, Glostrup, Denmark). Peroxidase labeling was revealed (1 to 10 minutes according to the antibody) in a dark chamber using 3,3-diaminobenzidine tetrahydrochloride (Sigma-Aldrich) with hydrogen peroxide in buffered solution (PBS). To exclude nonspecific binding, controls were carried out by omitting the primary antibody.

Phalloidin staining

Lower jaws of PN3 WT and *Cldn16*^{-/-} littermate mice ($n = 6$ per group) were embedded in OCT compound before frozen sectioning. Phalloidin staining was performed using the Alexa Fluor 647 Phalloidin (Invitrogen) as F-actin probe. Seven-micrometer-thick undecalcified frozen tissue sections were prepared, defrozen, and treated for 1/200 phalloidin in 1× PBS for 10 minutes in a dark chamber at room temperature. The sections are rinsed twice with 1× PBS for 2 minutes, stained with 0.1 µg/mL Dapi solution for 10 minutes, and rinsed twice with 1× PBS for 2 minutes. Sections are mounted in Mowiol (Sigma-Aldrich) and observed with a Yokogawa csu X1 Spinning Disk coupled with a DMI6000B Leica microscope. Acquisitions were made with MetaMorph 7 software. Identical imaging settings were used for all acquisitions.

Total protein extraction from incisor

Intra-bony parts of the growing lower incisor were dissected from 3-month-old WT and *Cldn16*^{-/-} mice ($n = 10$ per group). The samples were homogenized in ice-cold extraction buffer (2 samples in 100 µL buffer: 50 mM Tris-HCl, pH 7.5, containing 5 mM EDTA, 0.9% NaCl, and 0.2% Triton X-100), supplemented with 1/100 Protease Inhibitor Cocktail Set V EDTA free (Calbiochem, La Jolla, CA, USA). The resulting homogenates were then briefly sonicated on ice (3 times 5 sec), cleared by centrifugation at 10,000g for 15 minutes at 4°C and stored at -80°C .

Western blot analysis

Homogenates (20 µg) were subjected to SDS-PAGE on 4% to 20% precast gels (Mini-PROTEAN TGX Precast Gels, Bio-Rad, Hercules, CA, USA) and transferred onto a nitrocellulose membrane (Bio-Rad). Membranes were incubated with anti-amelogenin (1/750) and anti-enamelin (1/500, Santa Cruz Biotechnology) antibodies overnight at 4°C . The membranes were incubated with a 1/1000 dilution of a peroxidase-linked anti-rabbit IgG (amelogenin) or anti-goat (enamelin) secondary antibody for 1 hour at room temperature and developed by means of BM Chemiluminescence Western Blotting Kit (Roche Diagnostics, Meylan, France). As a control for protein loading, the membranes were carefully washed and stripped with

stripping buffer (Pierce Chemical, Rockford, IL, USA) and processed with a rabbit monoclonal anti-GAPDH antibody (Epitomics, Burlingame, CA, USA). The relative intensity of bands was digitalized and quantified using Image J software.

Gel zymography

Homogenates (5 µg) were analyzed by casein zymography to identify MMP-20. Electrophoresis was carried out using a miniprotein II system (Bio-Rad). Samples ($n=6$ per group) were half-diluted in 1 M Tris, pH 6.8, containing 50% glycerol and 0.4% bromophenol blue, and gels were run under Laemmli conditions. Casein Zymograms were run on Novex 4% to 16% casein zymogels (Life Technologies, Carlsbad, CA, USA), incubated at 37°C for 48 hours in 50 mM Tris-HCl buffer, pH 7.5, containing 5 mM CaCl₂ to allow MMP activity. After electrophoresis, gels were washed twice (30 minutes each) in 200 mL 2.5% Triton X-100 under constant mechanical stirring and incubated in 50 mM Tris-HCl buffer, pH 7.5, containing 150 mM NaCl, 5 mM CaCl₂ and 0.05% Brij 35, for 24 hours at 37°C. Gels were stained with 0.25% Coomassie brilliant blue G-250 (50% methanol, 10% acetic acid) and destained appropriately (40% methanol, 10% acetic acid). Proteinase activity was evidenced as cleared (white) bands. Bands were digitalized and compared using Image J software.

In situ zymography

Lower jaws of PN3 WT and *Cldn16*^{-/-} littermate mice ($n=6$ per group) were embedded in OCT compound before frozen sectioning. Seven-micrometer-thick undecalcified frozen frontal sections were prepared. The casein (Sigma-Aldrich) fluorescein conjugate protein (concentration of 1 mg/mL) was used for in situ zymography as a substrate for MMP following. Serial frozen sections were air-dried for 10 minutes. DQ-casein was diluted at 1/20 in 1% (w/v) low gelling temperature agarose in PBS. The mixture was put on top of the sections and covered with a coverslip. 10 mM EDTA and 1 mM 1,10-phenanthroline (Sigma-Aldrich), two MMP activity inhibitors, were used as controls.⁽²⁵⁾ After the agar was gelled, the incubation was performed at 4°C overnight. Gels without DQ-casein were processed in the same way as described above as negative controls. Examination of the substrate lysis was assessed using 1× 81 microscope (Olympus) and 20× objective. Acquisitions were made with ORCA R2 (Hamamatsu, Hamamatsu, Japan). Identical imaging settings were used for all acquisitions. Intensity of fluorescence analyses was performed using ImageJ homemade routines (<http://imagej.nih.gov/ij/>). Same threshold levels were used for both WT and *Cldn16*^{-/-} cases.

pH measurement in the enamel matrix of the PN3 mouse incisor

The lower jaws of *Cldn16*^{-/-} mice and their littermate WT mice were collected at PN3 ($n=9$ per group), embedded in OCT without decalcification, and cut in the frontal axis in a cryostat at -20°C (CM 3050S, Leica, Nanterre, France) using the first cusp of the first molar (M1) as a landmark. Sections located at the same level ahead of M1 for *Cldn16*^{-/-} and WT mice were defrozen and treated for 15 minutes in a dark chamber at room temperature with 5 µM acid free BCECF (2',7'-Bis-(2-Carboxyethyl)-5-(and-6)-Carboxyfluorescein, Life Sciences) diluted in saline. Sections were rinsed three times with saline. Samples were transferred to

the stage of an inverted microscope (Axiovision A1, Carl Zeiss, Oberkochen, Germany). pH was measured with imaging-based, dual excitation-wavelength fluorescence microscopy: extracellular dye was excited alternatively at 500 and 440 nm with a light-emitting diode (Optoled, Cairn Research, Faversham, UK). Emitted light was collected through a dichroic mirror, passed through a 530 nm filter, and focused onto an EM-CCD camera (iXon, Andor Technology, Belfast, Ireland) connected to a computer. The measured light intensities were digitized with 14-bit precision (16384 gray level scale) for further analysis. For each sample, 28 adjacent regions of interest were analyzed and the mean gray was measured with the Andor IQ software (Andor Technology, Belfast, Ireland). Background fluorescence was subtracted from fluorescence intensity to obtain intensity of intracellular fluorescence. Extracellular dye was calibrated at the end of each experiment. Samples were treated by a BCECF-containing 100 mM HEPES-buffered saline solution. Three different calibration solutions, titrated to 6.3, 6.8, or 7.3, were used.

Enamel staining with GBHA and pH measurement in the adult mouse incisor

The lower incisors of 3-month-old littermate WT and *Cldn16*^{-/-} mice ($n=6$ per group) were carefully dissected from the alveolar bone and the enamel organ firmly pulled off with a sterile gaze. In each mouse, one tooth was used for GBHA staining and one for pH measurement.⁽²⁶⁾ For GBHA staining,⁽²⁷⁻²⁹⁾ each incisor was stained under permanent stirring at room temperature for 2 minutes by immersion in 10 mL solution containing 3.75% GBHA (Sigma-Aldrich) and 1.275% sodium hydroxide dissolved in 75% ethanol. Subsequently, the incisors were briefly rinsed in 75% ethanol, rinsed in absolute ethanol, and air-dried. For pH measurement, the incisors were treated for 5 minutes in a dark chamber at room temperature with 5 µM acid-free BCECF and processed as described above. pH measurements were performed as previously reported by Damkier and colleagues.⁽²⁶⁾

Micro-X-ray computed tomography (micro-CT) analysis

Mandibles from 3-month-old littermate WT and *Cldn16*^{-/-} mice ($n=6$ per group) were scanned using a high-resolution X-ray micro-CT device (Quantum FX Caliper, Life Sciences, Perkin Elmer, Waltham, MA, USA) hosted by the PIPA Platform, EA2496 (Montrouge, France). 3D acquisitions were performed with an isotropic voxel size of 20 µm (90 kV, 160 mA, 180s). Enamel volume was measured using the open-source OsiriX imaging software (v3.7.1, distributed under LGPL license, Dr A Rosset, Geneva, Switzerland) from stack of 2D images. Binary thresholds were applied to isolate the enamel from the surrounding tissue. Incisor enamel thickness was assessed by measuring enamel surface under M1 (mesial and distal roots) and under M2 (mesial and distal roots) from micro-CT images using CTAn software (Skyscan, Aartselaar, Belgium) as previously reported.⁽³⁰⁾

Nanoindentation analysis

Cross-section samples incisors from 3-month-old littermate WT and *Cldn16*^{-/-} mice were prepared by cutting the resin-embedded samples perpendicular to the sagittal axis of the jaw at the level of the mesial cusp of the first molar ($n=8$ per group). To achieve an appropriate flatness and surface quality for the nanoindentation experiments, all surfaces of the cross sections were grinded using a Presi Mecapol P230 polishing machine. For

the grinding procedure, SiC paper was applied starting with mesh size of 120, which was subsequently decreased to 4000. After cleaning, the nanoindentation measurements were performed using a G200 Nanoindenter (Agilent Technologies, Inc., Vista, CA, USA) equipped with a Berkovich-shaped diamond indenter tip. Samples were tested in dry condition. For all nanoindentation measurements, the displacement-controlled continuous stiffness mode (csm) technique was applied. In this mode, small oscillations of the indenter tip are superposed to the overall indenter displacement of the loading and unloading testing cycle. Using the csm mode allows determining material parameters such as hardness and Young's modulus values as a function of depth for the complete range of indentation. For the experiments, a maximum indentation depth of 3000 nm was chosen while the loading speed was set to result in a strain rate (averaged within the locally loaded sample region) of 0.05 1/s. Typically, 15 single indentation tests were performed for each of the specimen enamel to be investigated. A representative indentation depth of 500 nm was chosen for determining the nanoindentation data on hardness and Young's modulus (modulus of elasticity). This value was found well suitable to compare all different enamel samples while minimizing effects resulting from surface microstructure.

Scanning electron microscopy (SEM)

Cross sections at the level of the mesial cusp of the first molar from 3-month-old littermate WT and *Cldn16*^{-/-} mice were performed with a saw equipped with a diamond disk (Struers, Champigny sur Marne, France) under a continuous water spray for SEM analyses ($n=6$ per group). After thorough polishing, surfaces were cleaned with 5% sodium hypochlorite for 2 minutes, rinsed twice with distilled water, etched with 2% nitric acid for 10 seconds, and then thoroughly rinsed with distilled water. Gold sputter-coated surfaces were observed under a scanning electron microscope (Cambridge S260 SEM, Cambridge, UK), equipped with an Everhart-Thornley and BSE electron detector.

Energy-dispersive X-ray spectroscopy (EDX)

Cross-section sample incisors from 3-month-old littermate WT and *Cldn16*^{-/-} mice were performed with a saw equipped with a diamond disk (Struers) under a continuous water spray for EDX analyses ($n=8$ per group). Uncoated surfaces, as prepared for the nanoindentation, were observed under a scanning electron microscope (Zeiss Supra55VP), equipped with a VPSE detector, and EDX analyses system (EDAX Genesis). All samples were evaluated for Ca/P ratio (% atom).

Laser ablation-inductively coupled plasma mass spectrometry (LA-ICPMS)

LA-ICPMS was used for analyses of elemental composition, in particular to compare the magnesium concentration of WT and *Cldn16*^{-/-} mice ($n=3$ per group). For the laser ablation, a device LSX 213 from Cetac (Omaha, NE, USA) was used. The ICPMS was performed with the device Element XR from Thermo Fisher Scientific GmbH (Schwerte, Germany). The samples were prepared as for the nanoindentation and SEM. The enamel were precisely ablated by a Nd:YAG-Laser with wavelength of 213 nm and a spot diameter of 50 μm and analyzed in the ICPMS.

RT-PCR analysis

Cldn16 gene expression was analyzed after extraction of total RNA from PN3 molar germs for secretory ameloblasts ($n=6$ per

group). RNA extractions were performed using RNeasy Micro Kit (Qiagen, Venlo, Netherlands). An amount of 250 ng total RNA (Nanovue Plus, GE Healthcare Life Sciences, UK) was reverse-transcribed with (cDNA kit VersoTM, Thermo Fischer, Waltham, MA, USA). For semiquantitative RT-PCR, cDNAs were amplified with specific primer (Go Tag Hot Start polymerase, Promega, Fitchburg, WI, USA). The PCR cycles consisted of an initial preincubation step (94°C for 5 minutes), followed by 30 cycles of amplification (95°C for 5 seconds, 55°C for 5 seconds, 70°C for 10 seconds). cDNA expressions were compared with *Gapdh* expression using: forward primer 5'-GGT CTG GAC TGT GTG AAG TT-3' and reverse primer 5'-GGC ATA AGG GTA GTT CCT CT-3' for *Cldn16*, and forward primer 5'-TGT GTC CGT CGT GGA TCT GA-3' and reverse primer 5'-TTG CTG TTG AAG TCG CAG GAG-3' for *Gapdh*.

qPCR analysis

Enamel matrix gene expression *Enam* and *Amelx* were analyzed after extraction of total RNA from the last 4 mm of mandibular incisor (soft part) from 3-month-old littermate WT and *Cldn16*^{-/-} mice ($n=6$ per group). RNA extractions were performed using RNeasy Micro Kit (Qiagen). An amount of 200 ng total RNA (Nanovue Plus, GE Healthcare Life Sciences) was reverse-transcribed with (cDNA kit VersoTM, Thermo-Fischer). cDNAs were amplified with specific primers (Eurofins mwg operon, Ebersberg, Germany) in a SYBR Green PCR Master Mix (Roche, Basel, Switzerland). Each primer pair was chosen for best efficiency and controlled for specificity using forward primer 5'-TAG ACA CCA GAT AGA TCA TAG AGC-3' and reverse primer 5'-ATG ACA CAG TAC AGT GAG AGT CTT-3' for *Enam*, forward primer 5'-GAT GGC TGC ACC ACC AAA TC-3' and reverse primer 5'-CTG AAG GGT GTG ACT CGG G-3' for *Amelx*, and forward primer 5'-TGT GTC CGT CGT GGA TCT GA-3' and reverse primer 5'-TTG CTG TTG AAG TCG CAG GAG-3' for *Gapdh*. Quantitative real-time PCR (qPCR) analyses was carried out using LightCycler 480.⁽³¹⁾ The PCR cycles consisted of an initial preincubation step (95°C for 5 minutes), followed by 45 cycles of amplification (95°C for 5 seconds, 55°C for 5 seconds, 70°C for 10 seconds). *Gapdh* was used as housekeeping gene. Relative gene expression levels were estimated using the deltaCq method.⁽³²⁾

In situ hybridization (ISH) analysis

RNA extractions were performed using RNeasy Plus mini kit (Qiagen), and cDNAs were synthesized using the Verso cDNA synthesis kit (Thermo-Fischer). RNA probes were designed using SP6 and T7-tailed oligonucleotides for *Amelx* (forward primer 5'-GCA ACC AAT GAT GCC AGT TC-3' and reverse primer 5'-AGA GGC AGC TCA GGA AGA AT-3') and *Enam* (forward primer 5'-ATG TGG CCT GGT ACC AAA TG-3' and reverse primer 5'-CAT GGT GGT TGT GGA TAG GG-3'). Sense and antisense RNA probes were synthesized and labeled with Digoxigenin-UTP (Roche) using the Riboprobe Combination System SP6/T7 RNA Polymerase kit (Promega) following the manufacturer's instructions. Lower jaws of PN3 WT and *Cldn16*^{-/-} littermate mice ($n=3$ per group) were embedded in OCT compound before frozen sectioning. Twelve-micrometer-thick undecalcified frozen tissue sections were prepared and fixed in 4% PFA for 10 minutes. ISH was carried out according to standard protocols with sense probes as control.⁽³³⁾

Statistical analysis

Values were presented as means and standard deviations. Statistical tests were performed with XLSTAT (v7.5.3, Addinsoft

Software, New York, NY, USA). According to the normality of the distribution, unpaired *t* test or Mann-Whitney's test were used. Welch's *t* test was used when equal variance was not assumed. Statistical significance was set at $p \leq 0.05$.

Results

Identification of AI in patients with FHHNC

In this study, we were able to examine five unrelated patients with FHHNC owing to *CLDN16* mutations (Fig. 1A). These patients were referred by the national Reference Center for Rare Disorders of Calcium and Phosphorus Metabolism and the Reference Center of Children and Adult Renal Hereditary Disorders (MARHEA), or by the Oral Care Center for Inherited Diseases, Brasilia-Brazil. Their main clinical and biological characteristics are summarized in Table 1. Patient 1 presented

with leg bowing from the age of 1 year requiring two osteotomies of lower limbs. At the age of 13 years, she was referred to Robert-Debré University Hospital (Paris, France), where bilateral NC, hypocalcemia, hyperphosphatemia, low 1,25 dihydroxyvitamin D concentration, and hypomagnesemia were first diagnosed with an atypical bone phenotype (bowing of the leg, brachymetacarpy but no sequelae of rickets at the ribs and at the skull). AI was diagnosed at the age of 15 years. She is from a nonconsanguineous family, and *CLDN16* analyses showed that she is compound heterozygous for a novel frameshift variant inherited from the mother and a known missense mutation inherited from the father. Patients 2 and 3 have been previously described by Blanchard and colleagues.⁽²⁴⁾ Patient 2 had seizures at the age of 8 years, leading to the discovery of severe hypocalcemia, hypomagnesemia, HC, and NC; AI was diagnosed at the age of 26 years. In patient 3, NC was discovered at the age of 8 years during the workup of abdominal pain;

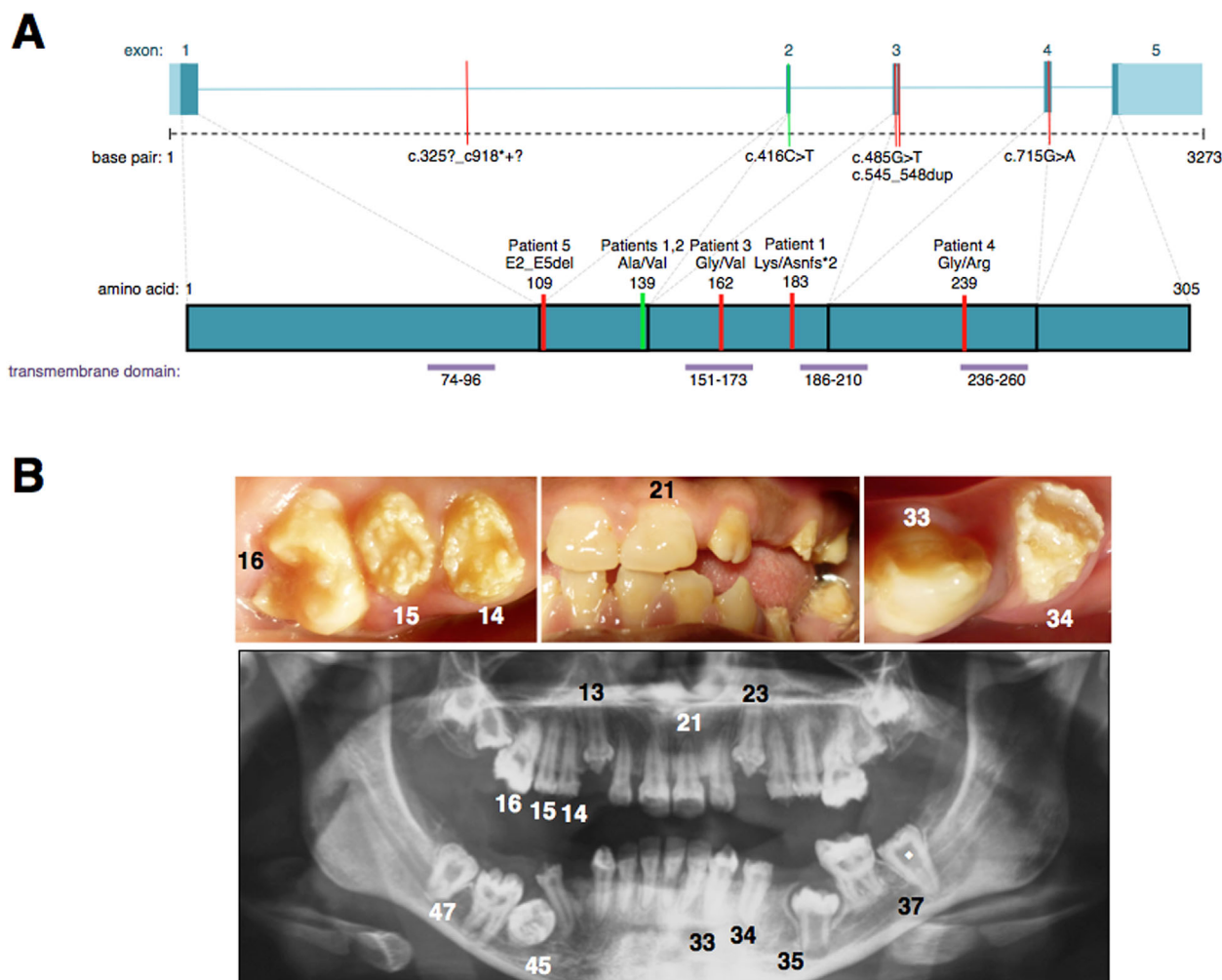


Fig. 1. *CLDN16* mutations of the studied patients and dental phenotype of patient 1. (A) The coding regions of *CLDN16* (NG_008149.1) are represented in dark blue and non-coding regions in light blue. The horizontal bars are introns. The mutations identified in the 5 patients are localized on the gene sequence as green and red vertical lines. Exons are associated by dotted lines to the schematic representation of the protein where corresponding mutations in the gene sequence are indicated as green and red vertical lines. (B) Clinical views and panoramic radiograph images from patient 1. The clinical crowns were shorter with hypoplastic and pitted enamel. Clinical views showed failed eruption, lateral infraclusion associated with abnormal swallowing. The panoramic radiograph highlighted multiple impacted teeth. The second molars showed concave occlusal surface without enamel. Pulp chamber enlargement (◆) was observed in the lower second molars.

Table 1. Renal and Oral Clinical Findings in 5 Patients With CLDN16 Mutations

Patient with FHINC	Sex	Year of birth	Height	Geographic origin	CLDN16 mutation ^a	Location on protein	Protein predicted function	Age at diagnosis of nephrocalcinosis (years)	Age at diagnosis of renal insufficiency (years)	Mg (mmol/L)	Urinary Ca (mmol/mmol creat)	Age at dental examination (years)	Type of AI	Impacted teeth
Compound heterozygous (no consanguineous)														
Patient 1 F		1996	115cm	Congo	c.416C>T	p.Ala139Val (inherited from the father)	Pathogenic (in silico) ^b	13	–	0.48	2.14	17	Hypoplasia (pitted enamel)	Yes
		-7.5 SD			c.545_548dup	p.Lys183Asnfs*2 (inherited from the mother)	Loss of function							
Patient 2 F		1988	158 cm	Morocco	c.416C>T	p.Ala139Val	Pathogenic (in silico) ^b	3	–	0.47	1	26	Hypoplasia (grooves)	Yes
Patient 3 F		1969	151 cm	Portugal	c.485G>T	p.Gly162Val	Pathogenic (in silico) ^b	8	16	0.39	0.52	45	Hypoplasia (grooves)	No
Patient 4 M		2008	+0.2 SD	Senegal	c.715G>A	p.Gly239Arg	Loss of function (in vitro confirmed) ^c	4	5	0.23	2.26	6	Hypoplasia (pitted enamel and grooves)	No
Patient 5 F		1988	163 cm	Brazil	c.325?_c918?+? (E2_E5del)	p.? (consanguineous)	Loss of function	20	20	0.37	2.7	20	Hypomaturation (mild)	No

^aSequences are numbered according to the cDNA sequence (GenBank accession number NM_006580.3). The A of the ATG initiator codon is denoted as nucleotide 1. Patients 1 and 2 have been described by Blanchard et al.⁽²⁴⁾; patient 5 has been described by Yamaguti et al.⁽³⁴⁾

^bSupplemental Table S1.

^cKonrad et al.⁽⁵⁸⁾; Hou et al.⁽²²⁾

hypomagnesemia and HC were first noticed at the age of 20 years. She currently has end-stage renal disease (on renal replacement therapy). AI was diagnosed at the age of 45 years. Patient 4 presented with an episode of gross hematuria at the age of 4 years; abdominal ultrasonography revealed bilateral NC and biological data showed hypomagnesemia and HC. At the age of 6 years, AI was diagnosed and renal function evaluation showed stage 2 chronic kidney disease (CKD). He is from a consanguineous family; accordingly, he is homozygous for a known missense mutation with in vitro confirmed pathogenicity.⁽²²⁾ Patient 5 is a Brazilian patient diagnosed with FHHNC, stage 3 CKD, and AI at the age of 20 years.⁽³⁴⁾ At 25 years, she reached end-stage renal disease and started dialysis. Her parents are first-degree cousins and she harbors a homozygous *CLDN16* deletion of exons 2 to 5 detected by multiplex ligation-dependent probe amplification (MLPA). Altogether, described and novel mutations detected in these patients are potentially pathogenic. They affect highly conserved residues and in silico analyses of nonexpressed in vitro missense mutations predict these changes as pathogenic (Supplemental Table S1). Furthermore, novel mutations (one frameshift and the large deletion) were not present in either the 1000 Genomes Project database (<http://browser.1000genomes.org/index.html>) or the NHLBI Exome Variant Server (EVS, <http://evs.gs.washington.edu/EVS/>) and could result in the production of unstable mRNAs or truncated proteins.

The dental examination revealed that all the patients presented enamel defects (Fig. 1, Supplemental Figs. S1 and S2, and Table 1), including demarcated and diffuse opacities, reduced amount of enamel with pitted defects, and/or horizontal grooves. According to the AI classifications,^(7,8) four had hypoplastic enamel (patients 1 to 4) and one had hypomaturation (patient 5). Noteworthy, several permanent teeth had failed to erupt in patients 1 and 2, with persistence of deciduous teeth in the latter. In these patients, cone beam computed tomography (CBCT) revealed reduced follicular space around unerupted teeth, indicating tooth ankylosis (Supplemental Figs. S1 and S2). However, unlike *FAM20A*-associated ERS,⁽¹⁴⁾ no gingival hyperplasia was observed in all the patients with *CLDN16* mutations, and X-ray examination revealed no pulp chamber stone or ectopic gingival calcification.

Enamel defects in *Cldn16*^{−/−} mice

Dental observations of 3-month-old *Cldn16*^{−/−} mice showed enamel fractures and coronal dentin exposition on molars, especially visible on the lingual cusps of the lower molars (Figs. 2A and 3A). Quantitative analyses from high-resolution micro-CT of mandible samples demonstrated a significant lower enamel volume in molars of *Cldn16*^{−/−} mice when compared with WT mice ($p < 0.001$; Fig. 2A). The phenotype change of the lower incisor, although less obvious than in the molars possibly owing to the continuously growing process, showed a delayed mineralization of enamel surface layer, resulting in a slightly lower enamel volume (Fig. 2B). Furthermore, the measure of the incisor enamel surface under M1 and M2 showed that enamel thickness was significantly lower in *Cldn16*^{−/−} under M2 (Fig. 2C). SEM analyses showed well-formed enamel rods in *Cldn16*^{−/−} and WT mice (Fig. 3A). Using EDX, no difference was detected for calcium content in the enamel of *Cldn16*^{−/−} and WT incisors and a similar calcium-to-phosphorus ratio was found (Fig. 3B). Because the detection of magnesium value was below or in the range of the detection limit for the EDX method, LA-ICPMS was

used and showed no difference between *Cldn16*^{−/−} and WT (1140153 ± 125797 versus 1002010 ± 147078 intensity [cps], respectively). However, nanoindentation analyses revealed a lower Young's modulus, which indicates higher enamel elasticity in *Cldn16*^{−/−} versus WT incisors ($p = 0.040$) (Fig. 3C).

CLDN16 is an integral component of secretory ameloblasts' TJ, and its absence in *Cldn16*^{−/−} mice impairs TJ structure

In the WT mice, *Cldn16* mRNA was found in the kidney as well as in the molar germ (Fig. 4A). Immunostaining of the incisor and molar germs revealed that CLDN16 protein was localized in the TJ at the apical end of secretory ameloblasts (Fig. 4B, C), where it colocalized with zonula occludens-1 protein (ZO-1) (Fig. 5A), but it was not detected in maturation ameloblasts (Supplemental Fig. S3B). As expected, CLDN16 was not found by immunostaining in *Cldn16*^{−/−} mice. However, ZO-1 staining appeared diffuse when compared with WT, suggesting alteration in the secretory ameloblasts' TJ in *Cldn16*^{−/−} mice (Fig. 5A). When comparing *Cldn16*^{−/−} and WT mice, no difference could be observed in either *Fam20A* or *Cldn19* gene expression in the ameloblasts (secretory and maturation) (Supplemental Fig. S4). Furthermore, histological staining showed that secretory ameloblasts were well polarized and elongated in the forming molar and incisor in both groups (Fig. 5A, Supplemental Figs. S3A and S5). TEM analyses of WT PN3 incisor showed TJ as adjoining ameloblast membranes converging to form a thin line at the distal end of the cells, giving a quilted appearance to the intercellular junction complex (Fig. 5B). The TJ structure appeared different in *Cldn16*^{−/−} secretory ameloblasts, with nonlinear and irregular structures (Fig. 5B). Furthermore, phalloidin staining of actin filaments, which are known to be associated with TJ,⁽³⁵⁾ was irregular in *Cldn16*^{−/−} incisor germs compared with WT (Fig. 5B). Altogether, these data indicate that TJ located at the apical end of secretory ameloblasts are impaired in *Cldn16*^{−/−} mice.

Consequences of CLDN16 deficiency on enamel matrix

We examined the effect of *Cldn16* knockout on the activity of the enamel-specific proteinase MMP-20⁽³⁶⁾ (enamelysin), which is known to be a major actor of early enamel maturation.^(37,38) In situ casein zymographic analyses of MMP-20, performed directly on PN3 incisor sections, clearly evidenced a significantly lower enzymatic activity ($p = 0.015$) in the enamel matrix of *Cldn16*^{−/−} mice when compared with WT (Fig. 6A; Supplemental Fig. S6A). However, similar expression amounts of this enzyme were revealed in the germ extracts by casein polyacrylamide gel zymography (Supplemental Fig. S6B), a biochemical method that measures protease total levels and activation state. Furthermore, immunohistochemistry for MMP-20 revealed a similar labeling in the enamel matrix of *Cldn16*^{−/−} and WT PN3 incisors (Supplemental Fig. S6B). Taken together, these data indicate that the reduced activity observed by in situ zymography in the *Cldn16*^{−/−} mice PN3 incisors is not because of defect in either enzyme synthesis or proform activation but rather to a change in the enamel matrix environment, which can inhibit MMP-20 activity.

Because proteinases activity is affected by pH,⁽³⁹⁾ we measured pH in the forming enamel matrix using the pH-sensitive dye BCECF. A significant lower pH value (6.79 ± 0.05 versus 7.08 ± 0.05 pH units, $p < 0.001$) was measured in the enamel matrix of *Cldn16*^{−/−} mice when compared with WT mice

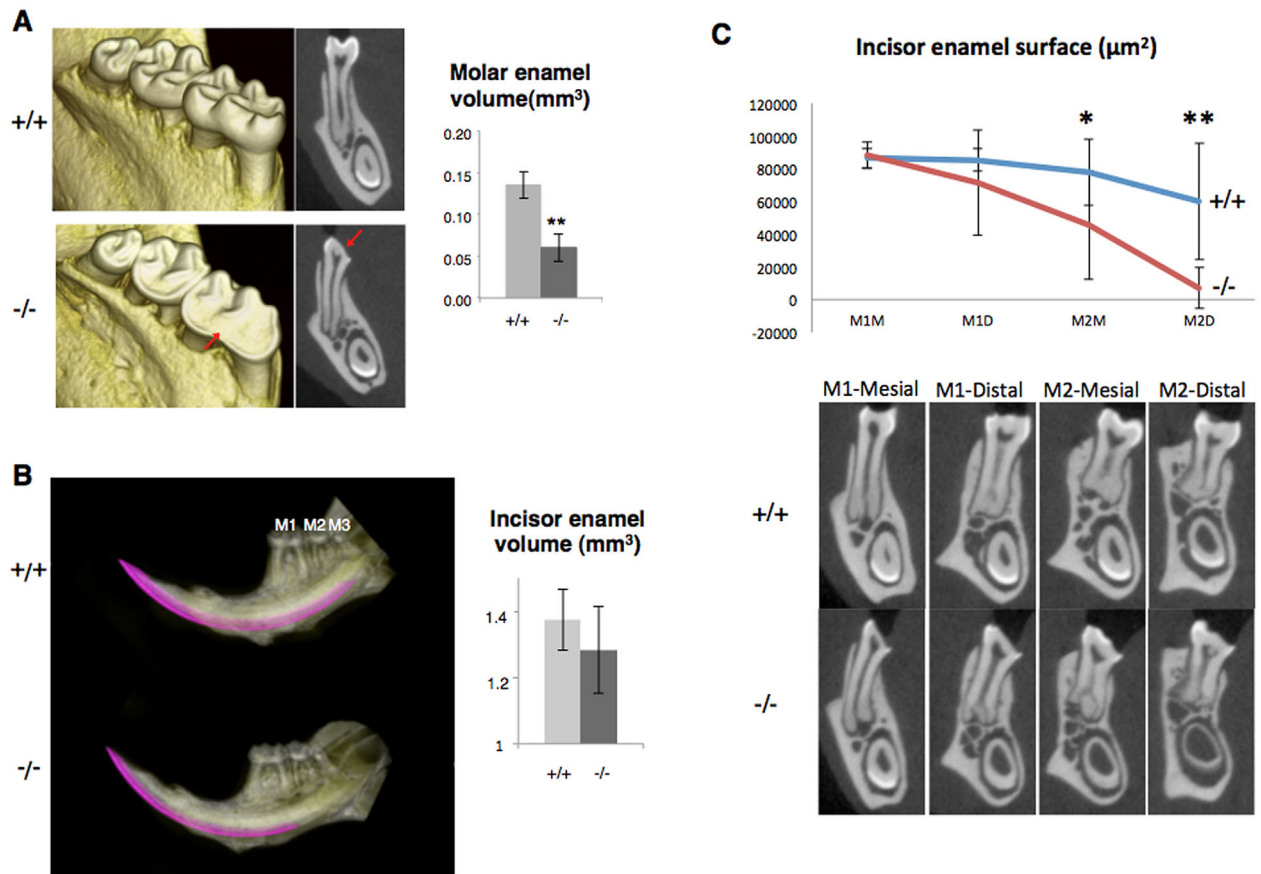


Fig. 2. Dental phenotype of 3-month-old *Cldn16*^{-/-} mice. (A) 3D volume rendering from micro-CT data and micro-CT sections showed severe enamel loss on lingual molar cusps in *Cldn16*^{-/-} mice (arrow). Quantitative analyses showed a significant lower enamel volume in *Cldn16*^{-/-} mice when compared with WT (0.061 ± 0.017 versus $0.136 \pm 0.016 \text{ mm}^3$, respectively, $p < 0.001$) ($n = 6$ per group). (B) Quantitative analyses from high-resolution micro-CT of mandible samples showed a nonsignificant lower enamel volume in incisors of *Cldn16*^{-/-} mice when compared with WT ($n = 6$ per group). In WT mice, incisor mineralization is observed under the third molar (M3), whereas in *Cldn16*^{-/-} mice it is detected under the second molar (M2). (C) Quantitative analyses from high-resolution micro-CT of mandible samples showed a significant lower enamel surface in incisors under M2 of *Cldn16*^{-/-} mice when compared with WT ($n = 6$ per group). * $p < 0.005$, ** $p < 0.0001$ WT versus *Cldn16*^{-/-} mice. M1 = first molar.

(Fig. 6B). We, therefore, sought to determine whether the modification in the proteolytic activity impaired the processing of enamel proteins in the *Cldn16*^{-/-} PN3 incisors. Western blot analyses of the protein extracts of the soft part of the growing incisor showed significantly higher levels of enamelin in *Cldn16*^{-/-} enamel; a similar, albeit nonsignificant, trend was found with amelogenin (Fig. 6C and Supplemental Fig. S7C), whereas no difference was observed in gene expression (Supplemental Fig. S7A, B). Therefore, our data suggest that the lower pH of the forming enamel matrix and the resulting decreased MMP-20 activity in *Cldn16*^{-/-} mice induced an accumulation of enamel proteins within the matrix.

We then assessed whether the absence of CLDN16 in *Cldn16*^{-/-} mice was associated with a lower pH also during enamel matrix maturation stage. GBHA staining showed two red bands, reflecting the position of smooth-ended maturation ameloblasts (SA).^(26,27,40) These bands had a similar profile in both the 3-month-old WT and the *Cldn16*^{-/-} mandibular incisors (Fig. 7). pH measurement across these bands using BCECF fluorescence clearly showed that the pH was significantly lower in the *Cldn16*^{-/-} enamel at the early part of the maturation zone (proximal band). It was similar in the distal band of both groups, albeit slightly lower in the central areas

in *Cldn16*^{-/-}. These data suggest that impaired amelogenesis in *Cldn16*^{-/-} mice may mainly result from locally disturbed pH control detected during enamel secretion and early maturation.

Discussion

A great interest has recently been given to kidney diseases associated with the dental disorder amelogenesis imperfecta (AI).^(13,41) Here, we described AI in 5 unrelated patients with the kidney disorder FHHNC owing to *CLDN16* mutations. The clinical observations of AI in our patients were supported by the dental examination of *Cldn16*^{-/-} mice, the mouse model of FHHNC, which, similarly to patients, displayed hypercalciuria and hypomagnesemia with normal concentrations of calcium and phosphorus in blood⁽²³⁾ and normal phosphorus level in urine (unpublished data). Adult *Cldn16*^{-/-} mice showed severe enamel loss, easily breakable enamel with underlying dentin exposure in molars, and decreased mineralization in continuously growing lower incisors. The altered dental phenotype of *Cldn16*^{-/-} mice may not be surprising in view of our demonstration that CLDN16 expression is not limited to the kidney as previously thought but is also localized in the TJ of

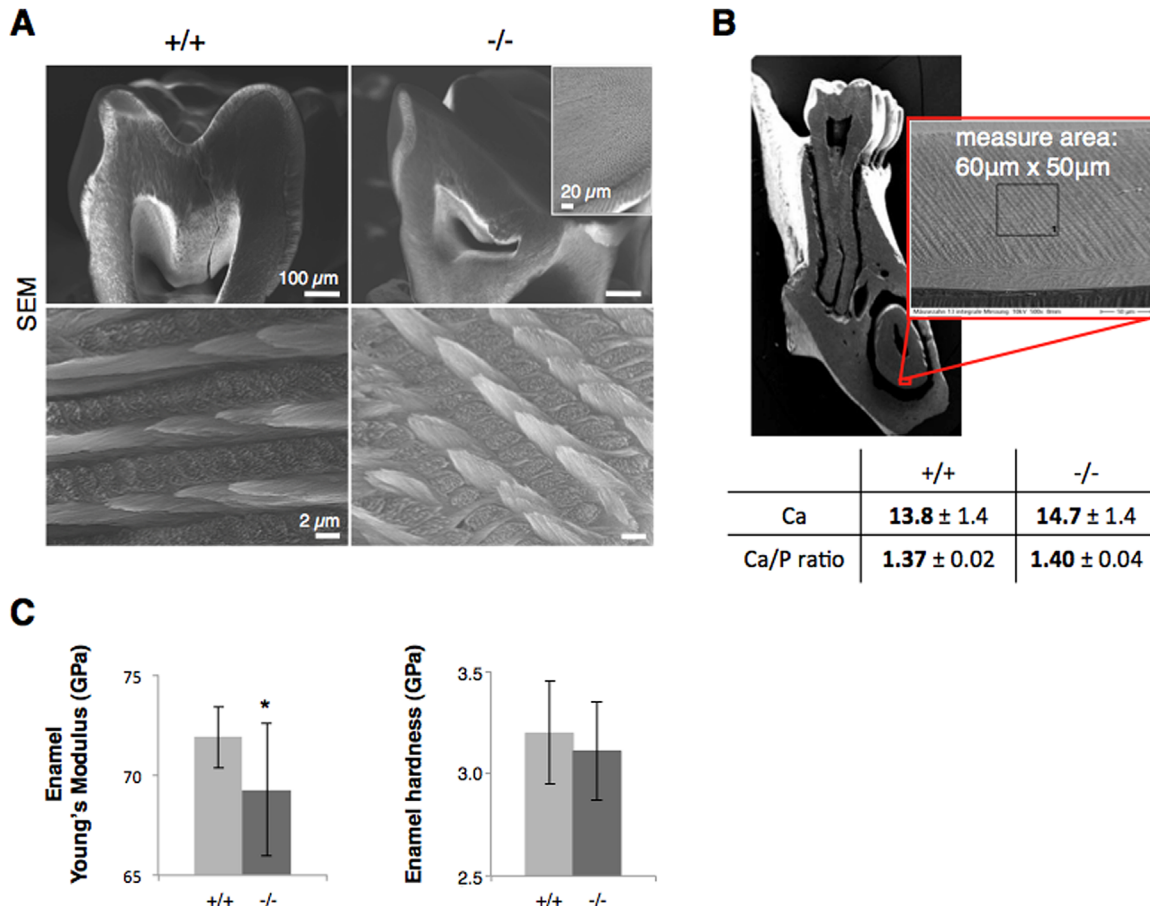


Fig. 3. Enamel structure analyses of 3-month-old *Cldn16*^{-/-} mice. (A) SEM analyses at the first molar (M1) level showed enamel loss and coronal dentin exposition in *Cldn16*^{-/-} molars when compared with WT. Enamel prisms seemed normally constituted in *Cldn16*^{-/-} incisor when compared with WT ($n = 6$ per group). (B) EDX analyses was performed on enamel of the incisor at M1 level and similar calcium (Ca) content and calcium-to-phosphorus (Ca/P) ratio were observed in *Cldn16*^{-/-} and WT mice ($n = 8$ per group). (C) Enamel analyses by nanoindentation of the growing lower incisor at the level of M1 showed a decrease in enamel Young's modulus (showing increased enamel elasticity) in *Cldn16*^{-/-} when compared with WT (69.3 ± 3.30 versus 71.9 ± 1.5 GPa, respectively, $p = 0.040$) ($n = 8$ per group). * $p \leq 0.05$, ** $p < 0.001$ WT versus *Cldn16*^{-/-} mice. No significant difference was observed in enamel hardness between *Cldn16*^{-/-} and WT mice ($n = 8$ per group).

secretory ameloblasts in the tooth germ. In addition, CLDN16 deficiency resulted in altered TJ structure in *Cldn16*^{-/-} mice. This suggests that the enamel defects observed in patients with FHHNC and *Cldn16*^{-/-} mice cannot be attributable only to the consequences of the kidney disease and the ensuing metabolic disorder but are also directly related to loss of function of CLDN16 within the forming enamel.

Despite the fact that all the mutations detected in our patients are predicted to be pathogenic (Table 1 and Supplemental Table S1), the enamel phenotypes of the 5 studied patients were variable, indicating that different stages of amelogenesis were affected. This phenotype heterogeneity may result from a combination of 1) altered TJ in secretory ameloblasts that affect enamel secretion and concomitant early maturation by MMP-20; 2) calcium and magnesium wasting ensuing from renal impairment early in childhood; and iii) age of onset of renal insufficiency. However, the fact that the latter two conditions were variable between our studied FHHNC patients (Table 1) and the findings that at least patients 1, 2, and 5 (who presented a late onset of the kidney

disease) did not present renal insufficiency during enamel formation but nevertheless had severe enamel defects are consistent with the idea that CLDN16 mutation is per se a direct cause of AI in these patients. Consistently, no dental abnormality has been described in patients with other causes of primary hypomagnesemia, particularly in patients with hypomagnesemia with secondary hypocalcemia caused by mutations of the *TRPM6* gene.^(42,43) However, low blood levels of calcium and vitamin D found in patient 1 may have contributed to the abnormal enamel formation in this particular patient, as enamel defects have been reported in patients with vitamin D-dependent rickets and in $1\alpha(OH)$ ase-null mice and VDR-null mice.⁽⁴⁴⁾

CLDN16 was detected in the TJ at the apical ends of secretory WT ameloblasts, where it colocalized with ZO-1.⁽⁴⁵⁾ TJ are known to create suitable microenvironments for enamel deposition and concomitant early maturation by determining the paracellular permeability and selectivity to solutes.^(45,46) Our data suggest therefore that, along with ZO-1 and F-actin filaments, CLDN16 is important for TJ assembly process and its loss impairs

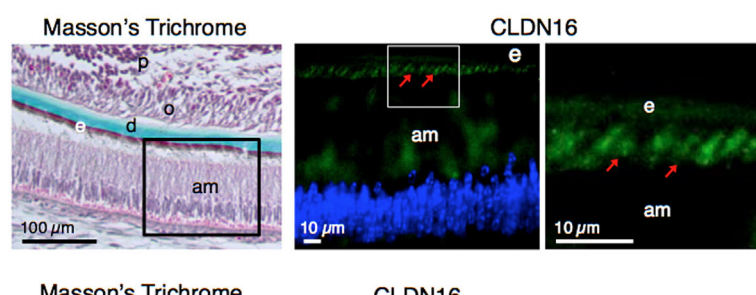
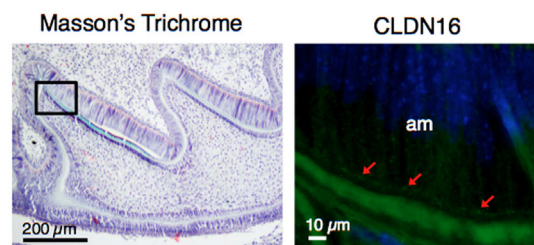
A**B****C**

Fig. 4. *Cldn16* expression profiling and identification of the protein in secretory ameloblasts. (A) *Cldn16* mRNA expression was analyzed in mouse tissues by RT-PCR. A representative gel image of the selected tissues shows *Cldn16* expression in mouse PN3 molar germ and kidney, whereas no mRNA was detected in bone, skin, liver, lung, and brain. (B) Identification of CLDN16 in the incisor by immunofluorescence. Masson's Trichrome staining of a sagittal section of PN3 WT incisor showing well-polarized ameloblast layer actively secreting enamel matrix. CLDN16 was expressed at the distal end of secretory ameloblasts (arrows) ($n=6$ per group). (C) Identification of CLDN16 in the PN3 molar germ by immunofluorescence. Masson's Trichrome staining of a sagittal section of PN3 WT molar germ showing the secretory ameloblast layer. CLDN16 was expressed at the distal end of secretory ameloblasts (arrows). am = ameloblasts; e = enamel matrix; o = odontoblasts; d = dentin; p = pulp.

TJ organization in secretory ameloblasts and consequently disturbs enamel formation.

In the kidney, CLDN16 is known to play a central role in reabsorption of divalent cations, but data on its exact mechanism of action are still conflicting.^(1,23) Of note, our data suggest that lack of CLDN16 in the tooth may not impair calcium transport across the epithelium because the Ca/P ratio in enamel appears not altered in *Cldn16*^{-/-} mice. The absence of CLDN16 in the secretory ameloblasts resulted in a significantly lower pH in the forming enamel matrix. This lower pH in enamel matrix did not result from systemic acidosis *Cldn16*^{-/-} mice because serum pH was similar in both *Cldn16*^{-/-} mice and WT (Supplemental Fig. S8), suggesting that it resulted from impaired local pH regulation.

The proteolytic activity of MMP-20 during early enamel maturation was shown to be critically dependent on pH values because the ability of MMP-20 to degrade amelogenin substrate at pH 6.4 or pH 8 was almost negligible when compared with that observed at pH 7.2.⁽⁴⁷⁾ The drastic effect of pH reported in

this study suggests that even the smaller drop of pH observed here (6.8 versus 7.1) is expected to result in a significantly lower MMP-20 activity within the enamel matrix of the *Cldn16*^{-/-} mice. We further report that the lower MMP-20 activity observed in the *Cldn16*^{-/-} forming enamel is associated with the accumulation of enamel matrix proteins, as supported by Western blot analyses and the delay of mineralization observed in the continuously growing incisor. Alterations in these proteins have been shown to affect enamel formation. Amelogenin or enamelin gene mutations were identified in patients with AI with varying clinical phenotypes.^(48,49) Furthermore, altered levels of enamelin were shown to impair enamel production.⁽⁵⁰⁾ Taken together, these data suggest that CLDN16 loss of function, by modifying environmental factors such as pH, impairs the processing of enamel matrix proteins and disturbs enamel formation, explaining the defects observed both in patients with FHHNC and in *Cldn16*^{-/-} mice.

The importance of a tight control of the extracellular pH on enamel mineralization has been previously emphasized.^(51,52)

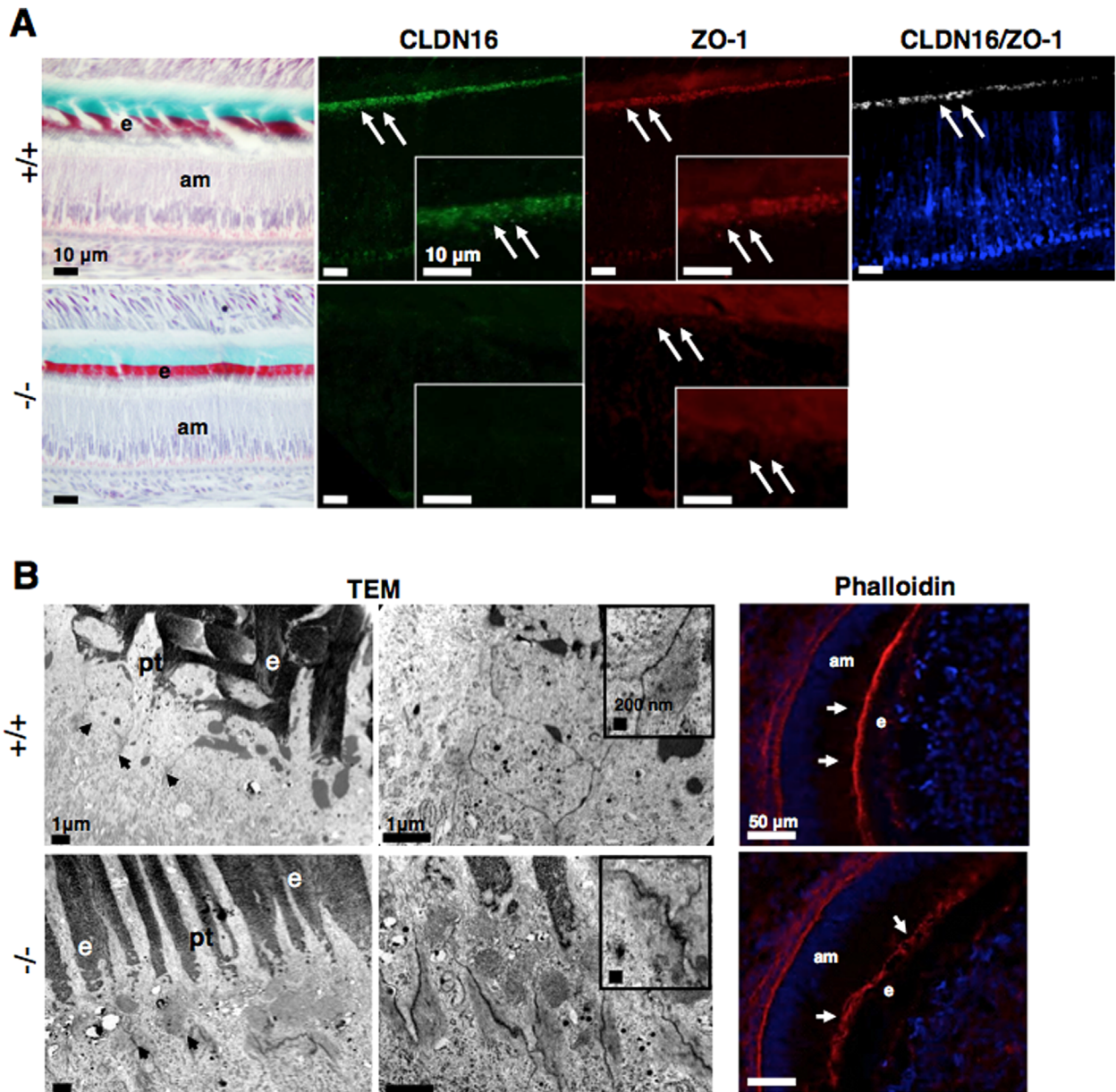


Fig. 5. Analysis of secretory ameloblast intercellular junctions in *Cldn16*^{-/-} mice. (A) Masson's Trichrome staining of sagittal sections of PN3 incisor showing secretory stage ameloblasts (am) associated at their apical end with the forming enamel matrix (e) stained in red, in *Cldn16*^{-/-} and WT mice. Ameloblasts appeared polarized in both groups with nucleus located at the basal end of the cells. CLDN16 protein was localized at the apical end (arrows) of secretory ameloblasts in WT mice, whereas no signal was observed in *Cldn16*^{-/-} mice. The TJ-associated protein zonula occludens-1 (ZO-1) was localized at the apical end (arrows) of the cells. ZO-1 labeling appeared more diffused in the *Cldn16*^{-/-} mice. CLDN16 colocalized with ZO-1 protein in WT mice (arrows). No colocalization was observed in *Cldn16*^{-/-} mice using identical imaging settings in the two panels ($n = 6$ per group). (B) Imaging by TEM at the apical end of secretory ameloblasts of *Cldn16*^{-/-} and WT mice. The adjoining cell membranes in WT mice converged to form a thin line (arrows) in contrast to nonlinear, thicker, and packed structures in *Cldn16*^{-/-} mice (arrows) ($n = 3$ per group). Phalloidin staining of the F-actin filaments located at the distal end (arrows) of ameloblasts showed a linear and continuous network in WT compared with an irregular and disrupted organization in *Cldn16*^{-/-} mice ($n = 6$ per group). pt = Tomes' process.

Mutations of SLC4 family bicarbonate transporters expressed by ameloblasts (eg, AE2 and NBCe1) result in altered enamel structure in mice and humans.^(51,53,54) Recent analyses have demonstrated that repeated pH cycling during the maturation stage allowed the progressive formation of enamel made of near-perfect hydroxyapatite crystals.⁽²⁶⁾ Phenotype modulation

between ruffle-ended (RA) and SA ameloblasts was shown to be associated with removal and restoration of their apical TJ, a mechanism that has been proposed to contribute to local extracellular pH cycling.⁽¹⁸⁾ The lack of CLDN16 protein did not prevent pH cycling but lowered the pH value of the enamel surface. Our finding that the lower pH in *Cldn16*^{-/-} mice was

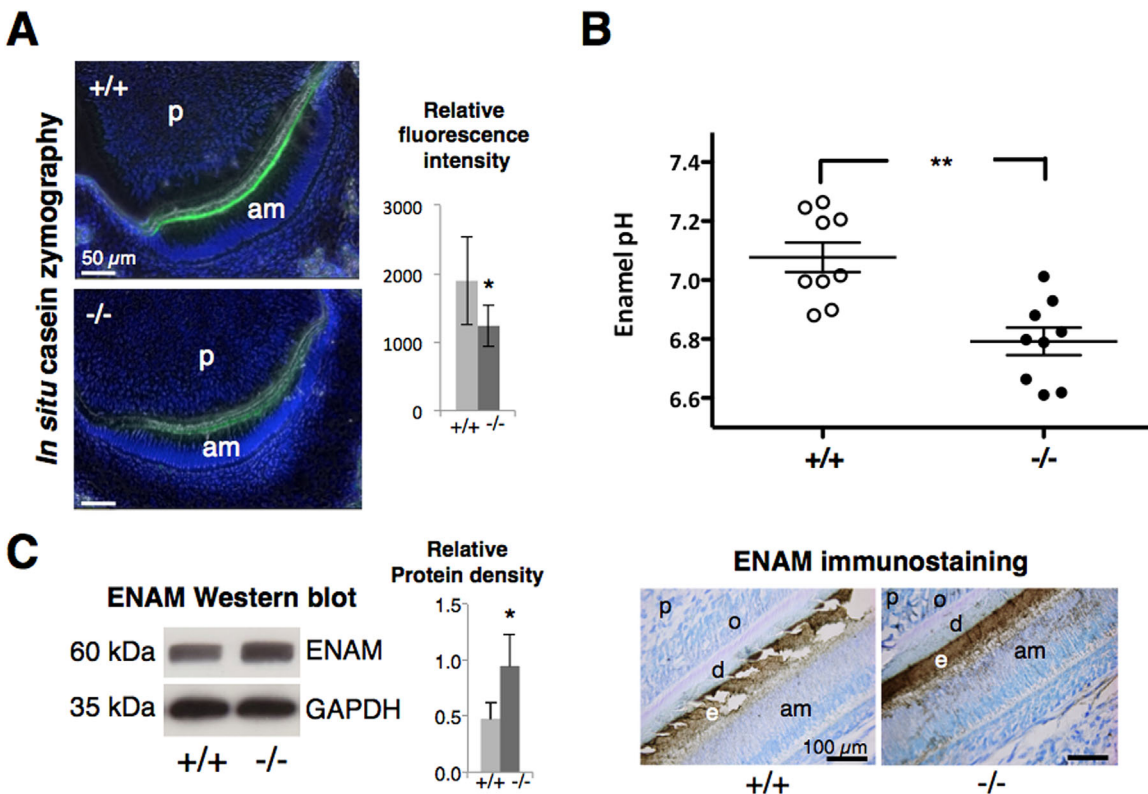


Fig. 6. Consequences of *Cldn16* mutation on enamel. (A) *In situ* casein zymographic analyses on PN3 incisor frontal sections showed a decreased enzymatic activity in *Cldn16*^{-/-} when compared with WT enamel (relative intensity: 1233 ± 303 in *Cldn16*^{-/-} versus 1895 ± 645 in WT, $p = 0.015$) ($n = 6$ per group). (B) pH values in the forming enamel matrix associated with secretory ameloblasts were lower in PN3 *Cldn16*^{-/-} incisors than in WT (6.79 ± 0.05 versus 7.08 ± 0.05 pH units, $p < 0.001$) ($n = 9$ per group). (C) Consequences of the mutation on enamel protein expression. Western blot analyses showed that enamelin (ENAM) was significantly increased in *Cldn16*^{-/-} mice ($p = 0.05$; $n = 10$ per group). Enamelin immunostaining showed a stronger labeling in the forming enamel matrix of *Cldn16*^{-/-} mice when compared with WT ($n = 6$ per group). am = ameloblasts; e = enamel matrix; o = odontoblasts; d = dentin; p = pulp. * $p \leq 0.05$; ** $p < 0.001$ WT versus *Cldn16*^{-/-} mice.

measured in the proximal part of the maturing incisor (less mature), but not in the more distal (more mature) part of the tooth, may explain the attenuated enamel defects found in the continuously growing incisor. Moreover, the fact that CLDN16 protein was detected in the apical TJ of secretory ameloblasts but not of maturation ameloblasts supports the importance of CLDN16 to set the pH gradient across the ameloblast layer during the secretory and early maturation stages.

Recent studies have deciphered ion transporters expression in secretory and maturation ameloblasts and unraveled their role in the cycling of pH necessary for normal enamel formation.^(55,56) Further thorough molecular studies are mandatory to understand the mechanisms responsible for the lower enamel pH in the *Cldn16*^{-/-} mice and whether it involves changes in TJ function as previously shown for claudin-18 deficiency in the stomach⁽⁵⁷⁾ or changes in the expression of plasma membrane transporters.

In conclusion, this study reports enamel abnormalities in patients with FHHNC owing to *CLDN16* mutations, disclosing for the first time a defect in a TJ protein as a cause of a dental disorder. The examination of more patients with *CLDN16* mutations will be necessary to establish a reliable genotype/phenotype association. Assessing whether patients harboring mutations in genes encoding other TJ proteins or ion

transporters present in AI also appears mandatory. Our study also suggests that a professional dental examination of patients affected by renal disorders should become a standard to accelerate proper molecular diagnosis, phenotyping, and appropriate care.

Disclosures

All authors state that they have no conflicts of interest.

Acknowledgments

We thank Jérémie Sadoine (EA2496 and PIPA, Paris Descartes University, France) for his help producing micro-CT data; Stefanie Wahl and Sylke Meyer (Fraunhofer Institute for Mechanics of Materials IWM, Germany) for their help producing LA-ICPMS data; Plateforme Génomique (INSERM U1016, Paris, France) for their help producing qPCR data; Prof Lionel Moisan (UFR de Mathématique, Paris Descartes University, France) for his help with biostatistics; Lydie Cheval (INSERM UMRS 1138, Cordeliers Research Center, Paris-Diderot, Pierre et Marie Curie and Paris Descartes Universities, CNRS ERL 8228, Paris, France) for measuring blood pH in mice; and Gilles Carpentier for imaging sessions (CRRET, Paris-Est University, France). We thank

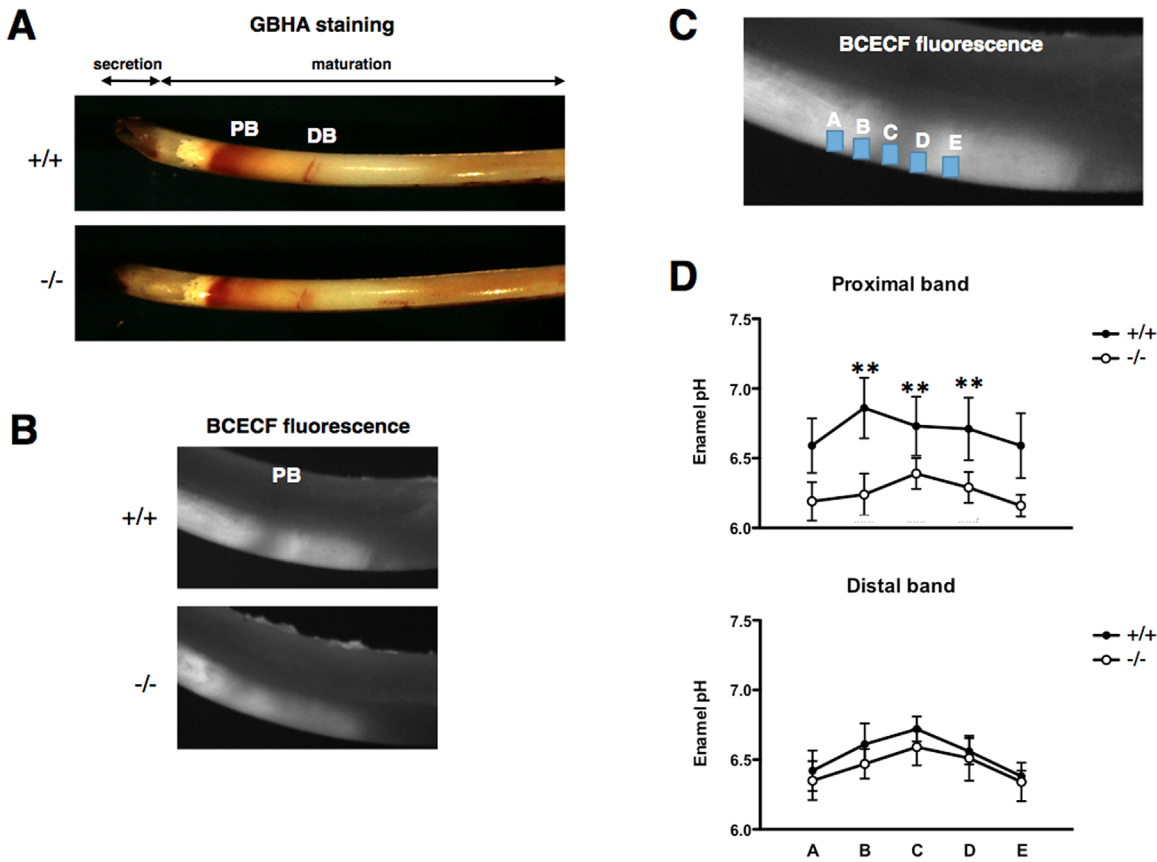


Fig. 7. pH measurement in maturation zone enamel. (A) Labial views of lower incisors stained with GBHA showing a proximal band (PB) and a distal band (DB) in the maturation zone of 3-month-old littermate WT and *Cldn16*^{-/-} mice ($n = 6$ per group). These bands correspond to the region of smooth-ended (SA) maturation ameloblasts. (B) Opposite lower incisors of WT and *Cldn16*^{-/-} mice treated with the fluorescent dye BCECF. (C) For each band, pH values were measured in the 5 areas A–E indicated in the upper panel by the squares according to Damkier and colleagues.⁽²⁶⁾ (D) Graphs showing the distribution of pH values across the SA bands. In the proximal band (close to the secretory stage), a significant lower pH was measured in *Cldn16*^{-/-} mice in B, C, and D areas. In the distal band, no significant difference was detected between WT and KO. ** $p < 0.001$ WT versus *Cldn16*^{-/-} mice.

Prof Marc McKee (McGill University, Canada) and Prof Yoshiro Takano (Tokyo Medical and Dental University, Japan) for their help regarding the study of enamel maturation stage.

This work was supported by grants from Paris Descartes University, from Fondation pour la Recherche Médicale for EA2496 and PIPA (FRM DGE2011123012), and the grant IDEX Sorbonne Paris Cité “Once upon a tooth.” YW (postdoctoral position) was supported by the French Chinese Foundation for Science and Applications (FFSCA), Académie des Sciences, and the China Scholars Council (CSC). DM and TB were supported by the Berlin Institute of Health. Parts of this study (nanoindentation, EDX, and LA-ICPMS) were financially supported by the Investitionsbank Sachsen-Anhalt, Germany (ZWB 1304/00006). CAPES-COFECUB supported PMY, AB, FN, and ACA.

Authors' roles: Study design: CB, AL, RVP, DM, PH, and CC. Study conduct: CC and PH. Data collection: CB, FC, WY, MK, BS, SR, JT, PMY, GR, MLF, TB, AGC, BV, DLM, BB, TG, AS, JMM, DB, GL, MM, JH, PCL, MCM, JCF, DT, RD, FN, DZ, AB, AK, MP, SM, AL, ACA, RVP, PH, and CC. Data analysis: CB, FC, WY, MK, BS, SR, PMY, AGC, TG, AS, GL, MM, AK, MP, SM, ACA, RVP, DM, PH, and CC. Data interpretation CB, FC, WY, SM, RVP, DM, PH, and CC. Drafting manuscript: CB, FC, SM, RVP, DM, PH, and CC. Revising manuscript content: CB, FC, BS, PMY, AB, AK, MP, SM, AL, ACA, RVP, DM, PH, and CC.

Approving final version of manuscript: CB, FC, WY, MK, BS, SR, JT, PMY, GR, MLF, TB, AGC, BV, DLM, BB, TG, AS, JMM, DB, GL, MM, JH, PCL, MCM, JCF, DT, RD, FN, DZ, AB, AK, MP, SM, AL, ACA, RVP, DM, PH, and CC. CC and PH take responsibility for the integrity of the data analysis.

References

1. Gunzel D, Yu AS. Claudins and the modulation of tight junction permeability. *Physiol Rev*. 2013;93(2):525–69.
2. Simon DB, Lu Y, Choate KA, et al. Paracellin-1, a renal tight junction protein required for paracellular Mg²⁺ resorption. *Science*. 1999;285(5424):103–6.
3. Hou J, Renigunta A, Gomes AS, et al. Claudin-16 and claudin-19 interaction is required for their assembly into tight junctions and for renal reabsorption of magnesium. *Proc Natl Acad Sci USA*. 2009;106(36):15350–5.
4. Weber S, Schneider L, Peters M, et al. Novel paracellin-1 mutations in 25 families with familial hypomagnesemia with hypercalciuria and nephrocalcinosis. *J Am Soc Nephrol*. 2001;12(9):1872–81.
5. MacGibbon D. Generalized enamel hypoplasia and renal dysfunction. *Aust Dent J*. 1972;17(1):61–3.
6. Lubinsky M, Angle C, Marsh PW, Witkop CJ Jr. Syndrome of amelogenesis imperfecta, nephrocalcinosis, impaired renal

- concentration, and possible abnormality of calcium metabolism. *Am J Med Genet.* 1985;20(2):233–43.
7. Wright JT. The molecular etiologies and associated phenotypes of amelogenesis imperfecta. *Am J Med Genet A.* 2006;140(23):2547–55.
 8. Poulsen S, Gjorup H, Haubek D, et al. Amelogenesis imperfecta—a systematic literature review of associated dental and oro-facial abnormalities and their impact on patients. *Acta Odontol Scand.* 2008;66(4):193–9.
 9. Crawford PJ, Aldred M, Bloch-Zupan A. Amelogenesis imperfecta. *Orphanet J Rare Dis.* 2007;2:17.
 10. Cetrullo N, Guadagni MG, Piana G. Two cases of familial hypomagnesemia with hypercalciuria and nephrocalcinosis: dental findings. *Eur J Paediatr Dent.* 2006;7(3):146–50.
 11. Jaureguiberry G, De la Dure-Molla M, Parry D, et al. Nephrocalcinosis (enamel renal syndrome) caused by autosomal recessive FAM20A mutations. *Nephron Physiol.* 2012;122(1–2):1–6.
 12. Wang SK, Aref P, Hu Y, et al. FAM20A mutations can cause enamel-renal syndrome (ERS). *PLoS Genet.* 2013;9(2):e1003302.
 13. Wang SK, Reid BM, Dugan SL, et al. FAM20A mutations associated with enamel renal syndrome. *J Dent Res.* 2014;93(1):42–8.
 14. De la Dure-Molla M, Quentric M, Yamaguti PM, et al. Pathognomonic oral profile of enamel renal syndrome (ERS) caused by recessive FAM20A mutations. *Orphanet J Rare Dis.* 2014;9(1):84.
 15. Kantaputra PN, Kaewgahya M, Khemaleelakul U, et al. Enamel-renal-gingival syndrome and FAM20A mutations. *Am J Med Genet A.* 2014;164A(1):1–9.
 16. O’Sullivan J, Bitu CC, Daly SB, et al. Whole-exome sequencing identifies FAM20A mutations as a cause of amelogenesis imperfecta and gingival hyperplasia syndrome. *Am J Hum Genet.* 2011;88(5):616–20.
 17. Cho SH, Seymen F, Lee KE, et al. Novel FAM20A mutations in hypoplastic amelogenesis imperfecta. *Hum Mutat.* 2012;33(1):91–4.
 18. Bartlett JD, Smith CE. Modulation of cell-cell junctional complexes by matrix metalloproteinases. *J Dent Res.* 2013;92(1):10–7.
 19. Smith CE. Cellular and chemical events during enamel maturation. *Crit Rev Oral Biol Med.* 1998;9(2):128–61.
 20. Ohazama A, Sharpe PT. Expression of claudins in murine tooth development. *Dev Dyn.* 2007;236(1):290–4.
 21. Godron A, Harambat J, Boccio V, et al. Familial hypomagnesemia with hypercalciuria and nephrocalcinosis: phenotype-genotype correlation and outcome in 32 patients with CLDN16 or CLDN19 mutations. *Clin J Am Soc Nephrol.* 2012;7(5):801–9.
 22. Hou J, Renigunta A, Konrad M, et al. Claudin-16 and claudin-19 interact and form a cation-selective tight junction complex. *J Clin Invest.* 2008;118(2):619–28.
 23. Will C, Breiderhoff T, Thumfart J, et al. Targeted deletion of murine Cldn16 identifies extra- and intrarenal compensatory mechanisms of Ca²⁺ and Mg²⁺ wasting. *Am J Physiol Renal Physiol.* 2010;298(5):F1152–61.
 24. Blanchard A, Jeunemaitre X, Couadol P, et al. Paracellin-1 is critical for magnesium and calcium reabsorption in the human thick ascending limb of Henle. *Kidney Int.* 2001;59(6):2206–15.
 25. Yamakoshi Y, Richardson AS, Nunez SM, et al. Enamel proteins and proteases in Mmp20 and Klk4 null and double-null mice. *Eur J Oral Sci.* 2011;119(Suppl 1):206–16.
 26. Damkier HH, Josephsen K, Takano Y, Zahn D, Fejerskov O, Frische S. Fluctuations in surface pH of maturing rat incisor enamel are a result of cycles of H⁽⁺⁾-secretion by ameloblasts and variations in enamel buffer characteristics. *Bone.* 2014;60:227–34.
 27. Takano Y, Crenshaw MA, Bawden JW, Hammarstrom L, Lindskog S. The visualization of the patterns of ameloblast modulation by the glyoxal bis(2-hydroxyanil) staining method. *J Dent Res.* 1982;Spec No: 1580–7.
 28. McKee MD, Warshawsky H. Modification of the enamel maturation pattern by vinblastine as revealed by glyoxal bis(2-hydroxyanil) staining and 45calcium radioautography. *Histochemistry.* 1986;86(2):141–5.
 29. McKee MD, Warshawsky H. Effects of various agents on staining of the maturation pattern at the surface of rat incisor enamel. *Arch Oral Biol.* 1986;31(9):577–85.
 30. Khaddam M, Huet E, Vallee B, et al. EMMPRIN/CD147 deficiency disturbs ameloblast-odontoblast cross-talk and delays enamel mineralization. *Bone.* 2014;66:256–66.
 31. Roche PC, Ryan RJ, McCormick DJ. Identification of hormone-binding regions of the luteinizing hormone/human chorionic gonadotropin receptor using synthetic peptides. *Endocrinology.* 1992;131(1):268–74.
 32. Pfaffl MW. A new mathematical model for relative quantification in real-time RT-PCR. *Nucleic Acids Res.* 2001;29(9):e45.
 33. Bardet C, Vincent C, Lajarille MC, Jaffredo T, Sire JY. OC-116, the chicken ortholog of mammalian MEPE found in eggshell, is also expressed in bone cells. *J Exp Zool B Mol Dev Evol.* 2010;314(8):653–62.
 34. Yamaguti PM, dos Santos PA, Leal BS, et al. Identification of the first large deletion in the CLDN16 gene in a patient with FHHNC and late-onset of chronic kidney disease: case report. *BMC Nephrol.* 2015;16: 92.
 35. Fanning AS, Ma TY, Anderson JM. Isolation and functional characterization of the actin binding region in the tight junction protein ZO-1. *FASEB J.* 2002;16(13):1835–7.
 36. Turk BE, Lee DH, Yamakoshi Y, et al. MMP-20 is predominately a tooth-specific enzyme with a deep catalytic pocket that hydrolyzes type V collagen. *Biochemistry.* 2006;45(12):3863–74.
 37. Bartlett JD, Simmer JP. Proteinases in developing dental enamel. *Crit Rev Oral Biol Med.* 1999;10(4):425–41.
 38. Lu Y, Papagerakis P, Yamakoshi Y, Hu JC, Bartlett JD, Simmer JP. Functions of KLK4 and MMP-20 in dental enamel formation. *Biol Chem.* 2008;389(6):695–700.
 39. Visse R, Nagase H. Matrix metalloproteinases and tissue inhibitors of metalloproteinases: structure, function, and biochemistry. *Circ Res.* 2003;92(8):827–39.
 40. McKee MD, Warshawsky H. Banding patterns in rat incisor enamel stained by histochemical complexing methods for calcium. *Anat Rec.* 1989;224(1):7–13.
 41. Martelli-Junior H, dos Santos Neto PE, de Aquino SN, et al. Amelogenesis imperfecta and nephrocalcinosis syndrome: a case report and review of the literature. *Nephron Physiol.* 2011;118(3):p62–5.
 42. Konrad M, Schlingmann KP. Inherited disorders of renal hypomagnesaemia. *Nephrol Dial Transplant.* 2014;29(Suppl 4):iv63–71.
 43. Lainez S, Schlingmann KP, van der Wijst J, et al. New TRPM6 missense mutations linked to hypomagnesemia with secondary hypocalcemia. *Eur J Hum Genet.* 2014;22(4):497–504.
 44. Foster BL, Nociti FH Jr, Somerman MJ. The rachitic tooth. *Endocr Rev.* 2014;35(1):1–34.
 45. Hata M, Kawamoto T, Kawai M, Yamamoto T. Differential expression patterns of the tight junction-associated proteins occludin and claudins in secretory and mature ameloblasts in mouse incisor. *Med Mol Morphol.* 2010;43(2):102–6.
 46. Inai T, Sengoku A, Hirose E, Iida H, Shibata Y. Differential expression of the tight junction proteins, claudin-1, claudin-4, occludin, ZO-1, and PAR3, in the ameloblasts of rat upper incisors. *Anat Rec (Hoboken).* 2008;291(5):577–85.
 47. Fukae M, Tanabe T, Uchida T, et al. Enamelysin (matrix metalloproteinase-20): localization in the developing tooth and effects of pH and calcium on amelogenin hydrolysis. *J Dent Res.* 1998;77(8):1580–8.
 48. Chan HC, Mai L, Oikonomopoulou A, et al. Altered enamelin phosphorylation site causes amelogenesis imperfecta. *J Dent Res.* 2010;89(7):695–9.
 49. Lee KE, Lee SK, Jung SE, et al. A novel mutation in the AMELX gene and multiple crown resorptions. *Eur J Oral Sci.* 2011;119(Suppl 1):324–8.
 50. Hu JC, Hu Y, Lu Y, et al. Enamelin is critical for ameloblast integrity and enamel ultrastructure formation. *PloS One.* 2014;9(3):e89303.
 51. Lacruz RS, Nanci A, Kurtz I, Wright JT, Paine ML. Regulation of pH during amelogenesis. *Calcif Tissue Int.* 2010;86(2):91–103.

52. Lyman GE, Waddell WJ. pH gradients in the developing teeth of young mice from autoradiography of [¹⁴C]DMO. *Am J Physiol.* 1977;232(4):F364–7.
53. Jalali R, Guo J, Zandieh-Doulabi B, et al. NBCe1 (SLC4A4) a potential pH regulator in enamel organ cells during enamel development in the mouse. *Cell Tissue Res.* 2014;358(2):433–42.
54. Demirci FY, Chang MH, Mah TS, Romero MF, Gorin MB. Proximal renal tubular acidosis and ocular pathology: a novel missense mutation in the gene (SLC4A4) for sodium bicarbonate cotransporter protein (NBCe1). *Mol Vision.* 2006;12:324–30.
55. Josephsen K, Takano Y, Frische S, et al. Ion transporters in secretory and cyclically modulating ameloblasts: a new hypothesis for cellular control of preeruptive enamel maturation. *Am J Physiol Cell Physiol.* 2010;299(6):C1299–307.
56. Lacruz RS, Smith CE, Kurtz I, Hubbard MJ, Paine ML. New paradigms on the transport functions of maturation-stage ameloblasts. *J Dent Res.* 2013;92(2):122–9.
57. Hayashi D, Tamura A, Tanaka H, et al. Deficiency of claudin-18 causes paracellular H⁺ leakage, up-regulation of interleukin-1beta, and atrophic gastritis in mice. *Gastroenterology.* 2012;142(2):292–304.
58. Konrad M, Hou J, Weber S, et al. CLDN16 genotype predicts renal decline in familial hypomagnesemia with hypercalciuria and nephrocalcinosis. *J Am Soc Nephrol.* 2008;19(1):171–81.